Journal of Power Sources 240 (2013) 745–752

Contents lists available at SciVerse ScienceDirect

Journal of Power Sources

journal homepage: www.elsevier.com/locate/jpowsour

Short communication

Polymeric ionic liquid nanoparticles as binder for composite Li-ion electrodes

Jan von Zamory [a], Mélanie Bedu [b], Sebastien Fantini [b], Stefano Passerini [a], Elie Paillard [a,*]

[a] Institute of Physical Chemistry, University of Muenster, Corrensstr. 28/30, 48149 Muenster, Germany
[b] Solvionic S.A., Site SNPE, Chemin de la Loge, 31078 Toulouse, France

HIGHLIGHTS

- Poly (ionic liquid) nanoparticles were obtained by dispersion polymerization.
- Poly (ionic liquid) nanoparticles were used as new binder for Li-ion battery electrodes.
- Graphite/Poly (ionic liquid) nanoparticles electrodes were cycled for more than 7 months.
- Practical performances were obtained for $Li_4Ti_5O_{12}$ electrodes incorporating the new binder.

ARTICLE INFO

Article history:
Received 4 February 2013
Received in revised form
22 April 2013
Accepted 25 April 2013
Available online 16 May 2013

Keywords:
Ionic liquid
Poly-ionic liquids
Li-ion electrodes
Latex binder
Li-ion battery
Nanoparticles

ABSTRACT

1-vinyl-3-ethylimidazolium bis(trifluoromethanesulfonyl)imide (VEIMTFSI) monomer was polymerized by dispersion polymerization in water in presence of an imidazolium-based ionic liquid crosslinker, leading to crosslinked polymeric ionic liquid nanoparticles. These nanoparticles were used as nanolatex binder to process Li-ion battery electrodes. Graphite electrodes were tested in half-cells vs lithium and showed excellent cycling performance for more than 7 months, although the irreversible capacity remained high in the initial cycles as compared with commercial electrodes. Sub-micrometric particles of ca. 200–300 nm of both carbon coated $LiFePO_4$ (LFP) and $Li_4Ti_5O_{12}$ (LTO) were also processed, leading to high coulombic efficiencies, although only the LTO electrodes allowed very stable cycling as well as practical performances.

1. Introduction

Ionic liquids (ILs), given their favorable properties such as high conductivity, good chemical and electrochemical stability, and negligible volatility [1], are now under investigation for use in many electrochemical energy conversion devices, such as dye sensitized solar cells [2], light emitting devices [3], electrochemical double layer capacitors [4] and lithium batteries [5], where they are mostly used as electrolytes. In the last years, polymers made of ionic liquid moieties (PILs) have also been investigated as solid polymer electrolytes for various applications [6–9].

Antonietti and Yuan [10] recently reported the dispersion polymerization of IL monomers in water and claimed that this kind of PILs could be used as binders. In their pioneering work, bromide-based ILs comprising alkyl-vinylimidazolium cations with alkyl chains lengths ranging from 8 to 18 carbons were used. Here, we report the direct synthesis by dispersion polymerization of ethyl-vinylimidazolium TFSI (VEIMTFSI), to form crosslinked PILs nanoparticles as well as their use as binder for Li-ion battery based on microsized graphite particles as well as sub-micrometric $Li_4Ti_5O_{12}$ (LTO) and $LiFePO_4$ (LFP) particles.

Working directly with TFSI-based ILs allows starting with very pure IL monomers without any halide contamination, which would be detrimental for use in Li batteries. Indeed, although it is possible to perform anion exchange after the polymerization takes place, at least for linear polymers, the substitution of the halide at the monomer stage allows for easier washing with water as compared to densely crosslinked and hydrophobic particles. Moreover, working with TFSI-based (thus hydrophobic) ILs allows obtaining nanoparticles with a smaller imidazolium-

* Corresponding author.
E-mail addresses: Elie.Paillard@uni-muenster.de, elie.paillard@live.fr (E. Paillard).

0378-7753/$ – see front matter © 2013 Elsevier B.V. All rights reserved.
http://dx.doi.org/10.1016/j.jpowsour.2013.04.127

based ionic liquid monomer, which was not reported so far. In fact, nanoparticles were only reported for alkyl chain longer than twelve carbons when using bromide based alkyl-vinylimidazolium ILs [10].

With the current trend of going nano (or at least submicro), and the challenges it brings, these nanolatexes could be used to replace the currently used latex suspensions, whose dimensions can be bigger than some of the active material particles reported in literature. Indeed, nanoactive particles can even be smaller than the conductive carbons commonly used, leading to the need for new approaches to make the 'nano' dream comes true, such as building efficient electron conductive secondary percolating networks [11]. The same problem stands for latex binders, as the commercially available styrene butadiene rubbers (SBR) range from 90 nm to 170 nm (JSR catalog 2013). Indeed, although soluble binders such as PVdF are, as a matter of fact, 'nano', the increased surface area of the active material particles imposes using high amounts of binder, which is not cost efficient and leads to increased slurry viscosities, which are already high as a result of the presence of nanoparticles.

Moreover, as latex binders act as 'glue points' between particles, it is possible to increase the number of such 'glue points' by decreasing the binder particle size, i.e., using the same amount of binder. Additionally, the use of an insoluble binder strongly reduces electrode cracking or exfoliation from current collectors caused by soluble binder retraction upon drying [12,13].

Thus, the nanolatex reported here opens new possibilities for solving problems linked with the processing of small particles into Li-ion battery electrodes, such as adhesion issues, cracking of electrodes upon drying, need for more binder.

In a first step, we report the use of PIL binder nanoparticles to prepare electrodes in combination with graphite microsized particles. It is well known that imidazolium based ILs have narrower electrochemical stability windows [14] as compared to quaternary ammonium based ILs [5,14–17], especially in reduction. Nevertheless, this instability, which is extremely detrimental when using imidazolium-based ILs in combination with low operating potential electrodes, can be taken advantage of, considering that with a non soluble crosslinked PIL, the reduction reactions are expected to occur at the interface between the nanoparticles and the other electrode components only, thus helping the adhesion of the binder to graphite by chemical bonding upon reduction. Additionally, some effect on the SEI formation could *a priori* be expected.

In a second step, sub-micrometric particles of $Li_4Ti_5O_{12}$ (LTO) of ca. 200–300 nm were used to illustrate the possibility of processing sub-micrometric particles and nanoPIL into usable electrodes, when working within the electrochemical stability window of the imidazolium ring. Finally, electrodes comprising sub-micrometric particles of $LiFePO_4$ (LFP) were prepared to test the binder in mild oxidative conditions.

2. Experimental

2.1. PIL and IL synthesis

2.1.1. PolyVIMTFSI-c

In a typical procedure, VEIMTFSI (Solvionic SA) shown in Fig. 1 was dispersed in deionized water (1 g in 20 mL) with 10 mol% of 1,4 butanediyl-3,3′-bis-1-vinylimidazolium di-bis(trifluoromethanesulfonyl)imide as a crosslinker (VIMTFSI-4-VIMTFSI) (Solvionic SA), shown in Fig. 1 and 100 mg of poly(vinylpyrrolidone) (PVP) was added to stabilize the emulsion as well as 15 mg of $K_2S_2O_8$ as a water soluble radical initiator. To remove any oxygen, the system was purged with argon for half an hour. The solution was then stirred at 70 °C for 24 h.

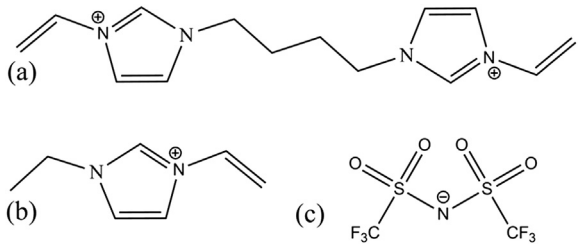

Fig. 1. Structural formula of (a) VIM^+-4-VIM^+, (b) $VEIM^+$ and (c) $TFSI^-$

The resulting particles were then centrifuged and the water eliminated. The rinsing procedure was repeated 8 times to ensure maximal purity and elimination of the PVP. This led to Poly-VIMTFSI-c under the form of a white powder. The polymer was then dried at 60 °C under vacuum for 24 h.

2.1.2. $Pyr_{14}TFSI$

N-butyl-N-methyl pyrrolidinium TFSI ($Pyr_{14}TFSI$) was synthesized using a procedure already reported [17], using freshly distilled bromobutane (99%, Acros), N-methylpyrrolidine (>99%, Fluka) and lithium bis(trifluoromethanesulfonyl)imide (3 M) as starting reagents. It was dried at 100 °C for 24 h using a turbomolecular pump to decrease the water content to less than 1 ppm.

2.2. Electrode preparation

The graphite electrodes were obtained by dispersing the dried PolyVIMTFSI-c in N-methylpyrrolidone under magnetic stirring. Graphite particles (SLP30, TIMCAL) were then added to reach a 90/10 wt% ratio. The resulting slurry was casted on copper current collector and dried for 24 h under vacuum either at 80 °C or 120 °C. The active mass loading was in the range of 1.5–1.9 mg cm^{-2}.

LTO and LFP electrodes were prepared in a similar way, with the addition of the conductive agent SuperC65 (TIMCAL), which leads to the following slurry formulation: 80 wt% LTO (Sachtleben-Hombitec LTO5) respectively $LiFePO_4$ (Süd-Chemie, carbon coated), 10 wt% SuperC65 and 10 wt% PolyVIMTFSI-c. The active material and the conductive agent were first grinded manually and subsequently added to the latex dispersed in NMP. After 24 h of magnetic stirring the slurry was casted on aluminum for LFP slurries and copper for LTO slurries. The active mass loading was in the range of 2.1–2.4 mg for LTO electrodes and 1.6–1.7 mg cm^{-2} for LFP electrodes.

The electrodes were punched in 12 mm diameter disks and dried for 24 h at 120 °C under vacuum and finally pressed at 8.85 ton cm^{-2} for 30 s.

2.3. Cell assembling

The cells were assembled in Swagelok™ three-electrode cells with lithium (Rockwood Lithium) counter and reference electrodes. Whatmann GF/D glass fiber discs wetted with either 1 M $LiPF_6$ in EC/DEC (3:7 v/v), battery grade (UBE), or or $Pyr_{14}TFSI$ (9:1 mol/mol) were used as separator and electrolyte. The cells where assembled in an argon filled glovebox with water and O_2 content inferior to 0.1 ppm. For the voltamperometry experiments, Ni was used as working electrode.

2.4. SEM

The polymer particles were investigated by high resolution scanning electron microscopy (SEM, AURIGA®, Zeiss).

2.5. Thermal analysis

Thermo-gravimetric measurements were carried out using a Q 5000 (TA Instruments). The samples were heated from room temperature to 500 °C at a heating rate of 10 K min^{-1} under either N_2 or O_2 flow. DSC experiments were done using a TA Instrument Q2000 DSC on samples in aluminum pans sealed in a dryroom (R.H. < 0.1%).

2.6. Electrochemical measurements

The cycling was done with a MACCOR Battery tester 4300. In the following, the terms charge and discharge refers to the half cells. For graphite electrodes, the discharge (lithiation) protocol consisted in a constant current (cc) step followed by a constant voltage (cv) step. The charge (delithiation) only included a cc step. The voltage limits were set to 20 mV (vs Li^+/Li) during discharge and 1.5 V (vs Li^+/Li) during charge for the graphite electrode. The constant voltage step limit was set to a current value lower than 1/100 of the current. For LTO and LFP electrodes, only cc steps were used, with respectively 1.2–2.2 V (vs Li^+/Li) and 2.8–4.2 V (vs Li^+/Li) cut-off potentials. The cyclic voltammetry tests were done at a sweep rate of 10 μV s^{-1} using a Solartron 1287 potentiostat.

2.7. FT-IR spectroscopy

IR spectra were acquired using a Bruker Vertex 70 FT-IR spectrometer.

3. Results and discussion

3.1. PIL nanoparticles characterization

In Fig. 2 are shown the nanoparticles of PolyVIMTFSI-c, with diameters around 40 nm for primary particles although some agglomeration can be seen on the SEM image displayed on Fig. 2.

The completeness of the polymerization reaction is confirmed by the FT-IR spectra showed on Fig. 3. The two bands corresponding to C–H bending in C=C–H disappear in the poly-VIMTFSI-c spectra. The C=C stretching region (not shown) is occupied by another band from the polymer.

The thermal stability of the polymerized material is high as seen on the TGA and DSC graphs (Fig. 4). Interestingly, no obvious features are observed on the DSC trace up to 150 °C while the TGA traces show no weight loss up to 200 °C both in N_2 and O_2 atmospheres. The 1 wt% weight loss is reached around 240 °C in both atmospheres.

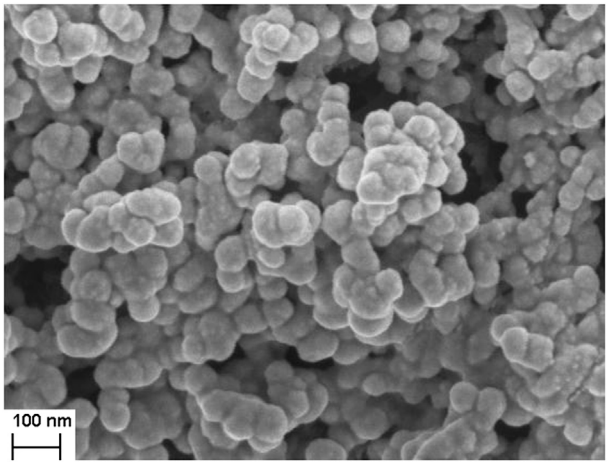

Fig. 2. SEM image of PolyVIMTFSI-c.

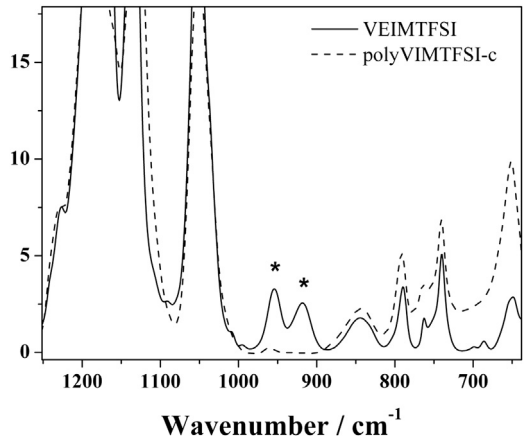

Fig. 3. FT-IR spectra of VEIM and PolyVIMTFSI-c.

3.2. Graphite electrodes characterization

The SEM images of the SLP30/PolyVIMTFSI-c electrodes (Fig. 5) shows a good dispersion of the particles upon electrode preparation (Fig. 5a) although the slurry was mixed using magnetic stirring. As seen on the Fig. 5b, the polymer particles adhere well onto the carbon surface, which might result from the use of polar NMP (see electrode preparation) that swells the binder nanoparticles (despite the expected high crosslinking density), thus helping the binder adhesion onto the carbon surface before being evaporated. As a matter of fact, mechanically stable electrodes where not obtained when using water as dispersion solvent, as the latter is unable to swell the hydrophobic particles. Thus, we suggest that the initial adhesion (prior to the first cycle) mechanism of the nanolatex is favored by the swelling, i.e., when the polymer is gelified, but is maintained after solvent removal, i.e., when the particles are stiff. This is very different from SBR latexes, which operates always above the polymer Tg.

On Fig. 5b, we can observe that the binder particles, although forming a monolayer on the surface of graphite are bound together to form flat aggregates partially covering the surface of the SLP30 particles. Fig. 5c shows that the polymer particles are not only present on the base plans, but also accumulate at the edges,

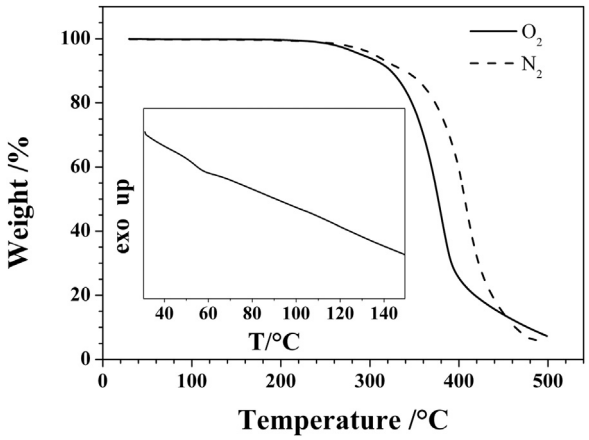

Fig. 4. TGA traces of the PolyVIMTFSI-c in N_2 and O_2 at 10 °C min^{-1}. Insert: DSC traces at 5 °C min^{-1}.

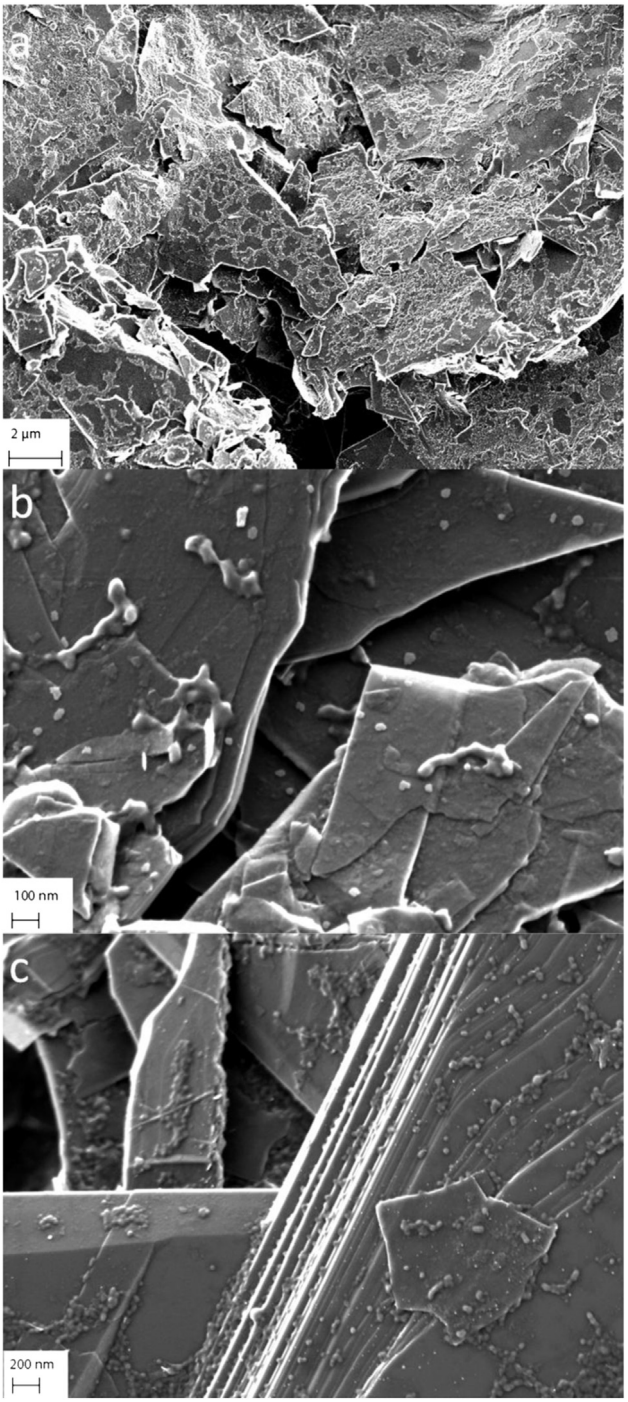

Fig. 5. SEM images of 90/10 (SLP30/PolyVIMTFSI-c) electrodes. (a) and (b) correspond to the same electrode, (c) shows another electrode obtained from a different batch of PolyVIMTFSI-c.

bridging different graphene layers together. Although not characterized further, this could somehow help preventing graphite exfoliation, due to the PIL binder particles acting as nano-stitches.

In Fig. 6 are reported the voltage profiles at C/10 for a few, selected charge/discharge cycles of a SLP30/PolyVIMTFSI-c electrode. First, the absence of a 1.2 V plateau in the first cycle, which would correspond to the reduction of the vinyl function of VEIMTFSI [18], is noticeable. Nevertheless, some irreversible reactions still occur such as the SEI formation taking place around 0.8 V, which is expected for EC containing electrolytes, as well as

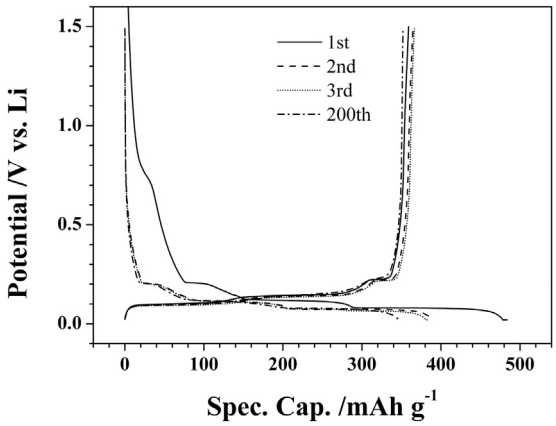

Fig. 6. Voltage profiles upon cycling at C/10 of a SLP30/PolyVIMTFSI-c (90/10) (wt/wt) electrode dried at 80 °C in 1 M $LiPF_6$ EC/DEC (3/7)(v/v) electrolyte. Counter and reference electrodes: Li.

possible further reductions of the imidazolium at lower potential. After the two initial cycles, the reversibility rises and almost no change is observed between the 3rd and 200th cycles.

To illustrate the different reduction peaks of VEIMTFSI (and by analogy of Poly-VEIMTFSI-c), Fig. 7 shows the voltammograms of pure $Pyr_{14}TFSI$ and $Pyr_{14}TFSI$ + 5%wt VEIMTFSI. The first peak, starting around 1.2 V vs Li^+/Li corresponds to the vinyl reduction as well as the α-H reduction between the N atoms of the imidazolium ring, leading to the formation of the imidazol-2-ylidene persistent carbene [19], as illustrated in Fig. 8, which occurs at lower voltage, but overlaps with the former peak. Two other electrochemical events occur at lower potentials, with onsets (indicated by stars in Fig. 7) at 0.6 V and 0.1 V vs (Li^+/Li), which overlap with the last stage of Li^+ intercalation into graphite and would correspond to further reduction steps of the imidazolium cation.

Fig. 9a shows that the cycling stability of electrodes dried at 80 °C at C/10 and 1C is very high and does not reveal obvious loss of active material particles for more than 240 cycles at C/10, which corresponds to more than 7 months of continuous cycling. Although the irreversible capacities in the initial cycles prevent so far the use of these electrodes in Li-ion batteries, it should be considered that this problem could be overcome either by ex-situ SEI formation or by reducing the binder content. At 1C, over 150 cycles were reached with minimal capacity fading. The average capacity decay (as referred to the highest reversible capacity reached) was 0.014% $cycle^{-1}$ at 1C and 0.023% $cycle^{-1}$ at C/10, both values being high for laboratory cells employing lithium metal counter electrodes. In fact, reduction products formed at the lithium metal electrode can diffuse

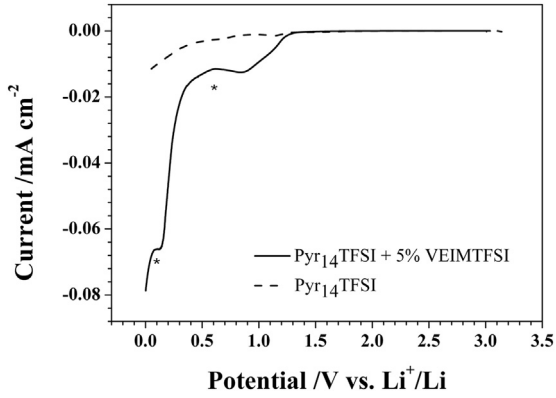

Fig. 7. Voltamperogram of $Pyr_{14}TFSI$ and $Pyr_{14}TFSI$ + 5%wt of VEIMTFSI. WE: Ni, reference and counter electrodes: Li. Scan rate 10 µV s^{-1}.

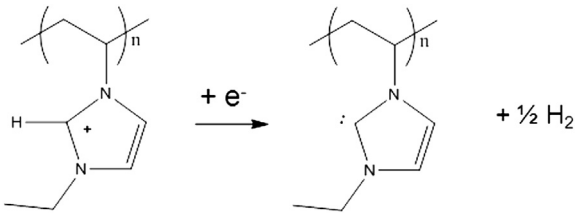

Fig. 8. Illustration of the reduction of PVIMTFSI-c to the associated imidazol-2-ylidene, according to reference [18].

to the graphite electrode and generate the thickening of the SEI, thus resulting in a decreased performance. The lowest fading at the highest C rate would be associated to the shortest overall test duration and the lower amount of reduction products generated at the lithium/electrolyte interface.

The coulombic efficiencies are also improved at 1C. Although this can be explained by the shorter test period, it might also originate from a better SEI formation. Indeed, the first cycles, efficiencies are rather low in both cases, but the efficiencies at 1C rise much faster as shown in Table 1. From the 5th cycle, the coulombic efficiencies are above 99% and rise further above 99.9%. This might be explained by the fact that multiple reactions are involved during SEI formation, as reduced species are further reduced or polymerized to form solid deposits. In case of a lower rate, some of the reduced species have the time to diffuse in the electrolyte instead of being further reduced and can then react in the following cycles, all

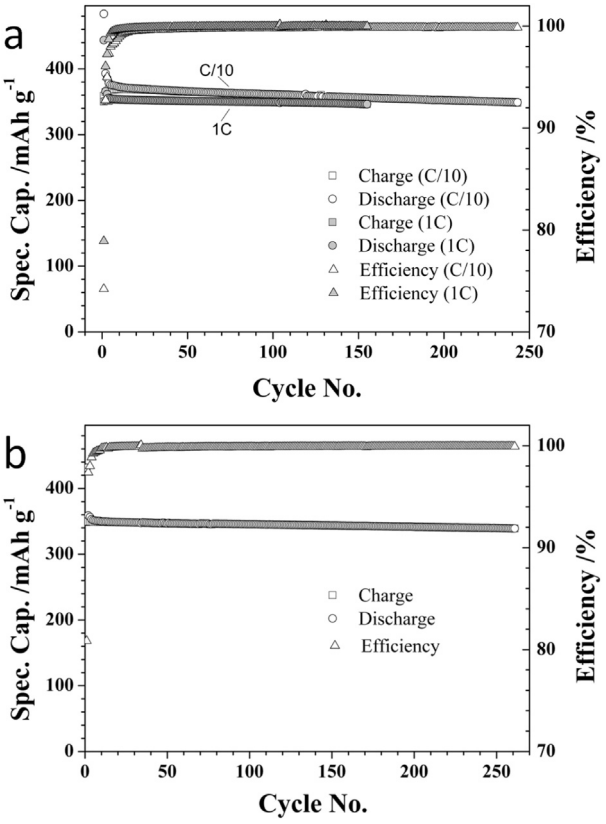

Fig. 9. Galvanostatic cycling (with additional constant voltage steps for lithiation (discharge)) of SLP30/PolyVIMTFSI-c electrodes. Electrolyte: 1 M $LiPF_6$ (EC/DEC) (3/7) (v/v). Counter and reference electrodes: Li. (a) Dried at 80 °C, at C/10 and 1C. (b) Dried at 120 °C, 3 cycles at C/10, 5 cycle at C/5, 5 cycles at C/2, 20 cycles at 1C then continuously C/10.

Table 1
Summary of the efficiencies at C/10 and 1C for SLP30/PolyVEIMTFSI-c electrodes dried at 80 °C and for an SLP30/PolyVEIMTFSI-c electrode dried at 120 °C at C/10.

Cycle number	Coulombic efficiency/%		
	C/10 (80 °C)	1C (80 °C)	C/10 (120 °C)
1st cycle	74.22	78.92	80.85
2nd cycle	92.73	96.06	97.39
3rd cycle	95.00	97.25	98.00
50th cycle	99.73	99.93	99.80
100th cycle	99.80	99.97	99.87
155th cycle	99.84	99.99	99.90

the more than the SEI is then less protecting. If we calculate the average irreversible capacity per cycle above the 50th cycle, we obtain 0.16% per $cycle^{-1}$ at C/10 and 0.033% $cycle^{-1}$ at 1C. These values, as well as the irreversible capacities in the first cycles could certainly be further increased by use of SEI forming additive such as vinylene carbonate (VC).

The ascertain the effect of the drying procedure, especially on the irreversible capacities of the electrodes, some electrodes were dried at 120 °C instead of 80 °C and as an example Fig. 9b shows the cycling at various C-rate (for the first 33 cycles then C/10 as indicated on the graph). C-rates up to 1C do not affect the capacity, although it has a clear effect on the irreversible capacity decay. Indeed, when comparing the efficiencies of the first three cycles at C/10 (Table 1), it appears that the higher drying temperature is highly beneficial.

To get a better idea of the irreversibility at C/10 and 1C over extended cycling and discriminate between irreversibility due to electrolyte reactivity vs lithium and the reactivity of the binder depending on the drying procedure, Fig. 10 shows the percentage of irreversible capacity per cycle for the 100 first cycles for two electrodes dried at 80 °C (at 1C and C/10) at and for the electrode dried at 120 °C with varying C-rates.

It appears that the drying procedure mainly influences the first cycles (as evidenced in Table 1), but then, mostly the C-rate determines the evolution of the efficiencies (although the electrode dried at 120 °C remains more efficient during the whole cycling test as compared to the two other electrodes at similar C-rates). Indeed, when switching to 1C, the electrode dried at 120 °C sees its irreversible capacities follow the curve of the 1C cell dried at 80 °C, while switching back to C/10 leads to an increase of the irreversible capacities as an effect of the lithium reactivity. Thus, it is possible to decrease the irreversible capacities down to around 0.02% (and below) per cycle at 1C whereas at C/10, a limit seems to be reached for both drying procedure at c.a. 0.2% of irreversible capacity per cycle.

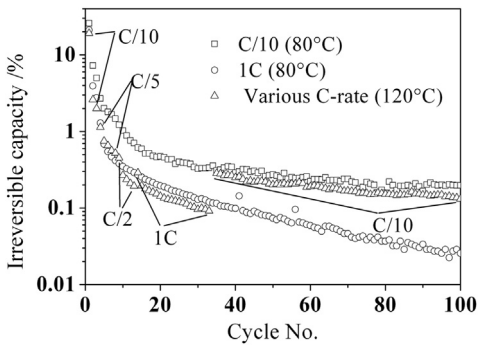

Fig. 10. Percentage of irreversible capacity per cycle for two electrodes dried at 80 °C at C/10 and 1C and for one electrode dried at 120 °C with C-rates indicated on the graph.

3.3. Submicrometric LTO electrodes characterization

Even though the irreversibility could certainly be reduced further by decreasing the amount of binder, it seems that the nanobinder could be used more efficiently with active materials operating within the electrochemical stability windows of the imidazolium cation. To assess the suitability of the PIL nanoparticles as binder for smaller particles, LTO particles of ca. 200–300 nm were processed with PolyVIMTFSI-c into electrodes. Fig. 11a reveals a good homogeneity of the electrodes, while Fig. 11b shows several bridging between LTO particles and the conductive carbon particles, which shows the good adhesion of the PIL on both components.

These electrodes led to improved efficiencies (95.1%, 99.5% for respectively the 1st and 2nd cycles and constantly above 99.9% from the 3rd cycle) as well as stable cycling at 1C (Fig. 12a) with minimum decay for more than 400 cycles, showing no contact loss and good binding properties. A C-rate test was performed on these electrodes up to 50C as shown on Fig. 12b. The graph shows strong capacity decay at 50C, which is likely due to electrolyte transport limitation, but interestingly, 100 mAh g^{-1} are reached at 20C. When switching back to 1C, the cell shows no influence of the higher C-rates used and cycle steadily.

3.4. Submicrometric LFP electrodes characterization

To test the suitability of the binder at higher potential, LFP electrodes were prepared, and the SEM images of the obtained

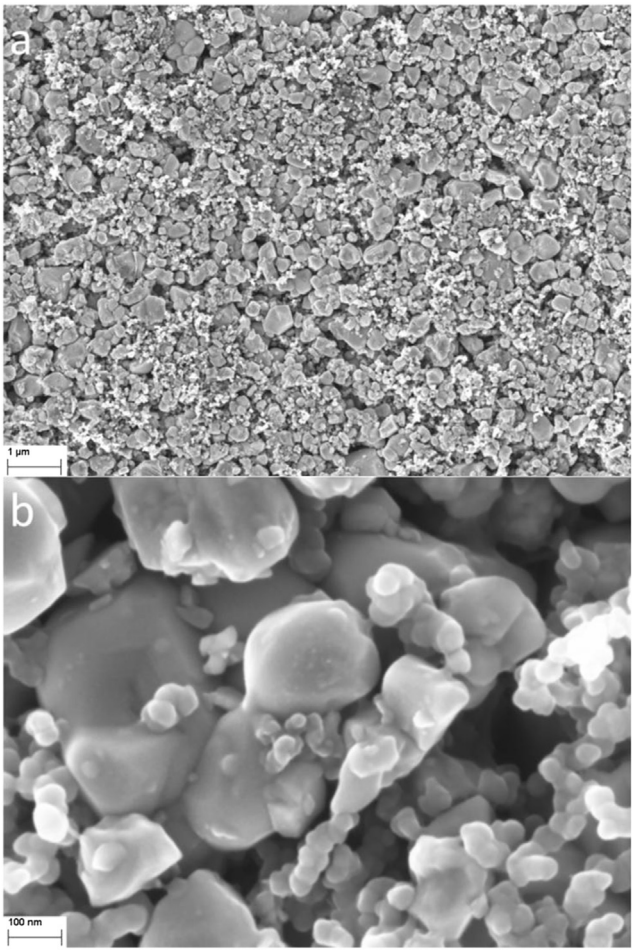

Fig. 11. (a) and (b): SEM images of a LTO electrode.

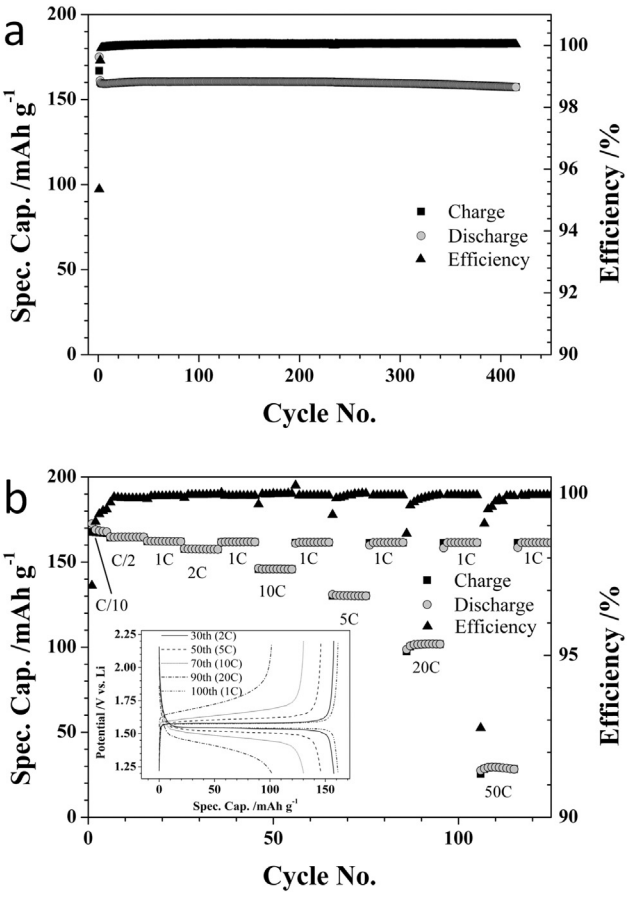

Fig. 12. Galvanostatic cycling of $Li_4Ti_7O_{12}$/SuperC65/PolyVIMTFSI-c electrodes (80/10/10 %wt) counter and reference electrodes: Li. (a) At 1C and (b) At various C-rates as indicated on the graph, with selected corresponding voltage profiles in insert.

electrodes are shown on Fig. 13a and b. On Fig. 13b, the presence of PIL on the surface of the LFP particles is not obvious, whereas some conductive agent particles seems to be agglomerated or bridged together by the PIL particles, which seems to have partially coalesced. The reason for that is not clear, considering that the LFP particles are carbon coated and that the PIL binder showed good adhesion on both graphite particles and conductive agent. Further processing, including ball-milling mixing did not lead to different feature within the electrodes.

The electrodes (comprising carbon additive) showed very promising reversibility in the first cycles, as shown in Fig. 13, reaching 99.8% in the second cycle, which results from the limited reactivity of the PIL in this voltage region (2.8–4.2 V vs Li^+/Li). Unfortunately, Fig. 14b shows an increasing irreversibility with cycling. One can see that after a few cycles, the efficiency starts dropping and after the C-rate test, the cycling at C/10 leads to low efficiency (90–92%) and finally, the cycling at 1C leads to rapid capacity decay and rather low (98%) coulombic efficiencies. Constant cycling at 1C from cycle one (not shown) also showed poor cycling stability (capacity decay after 20 cycles) and efficiencies decreasing from cycle 12.

The reason for this behavior is not clear, and possibly the processing of the electrodes was not successful, nevertheless, loss of contact would have led to a loss of capacity, but not necessarily to efficiency decay. An explanation could be that the cut-off voltage of 4.2 V vs Li^+/Li resulted in progressive loss of binding as a result of the oxidation of the PIL over time. As the capacity decay is accompanied by a strong decrease in efficiency, it is clear that over

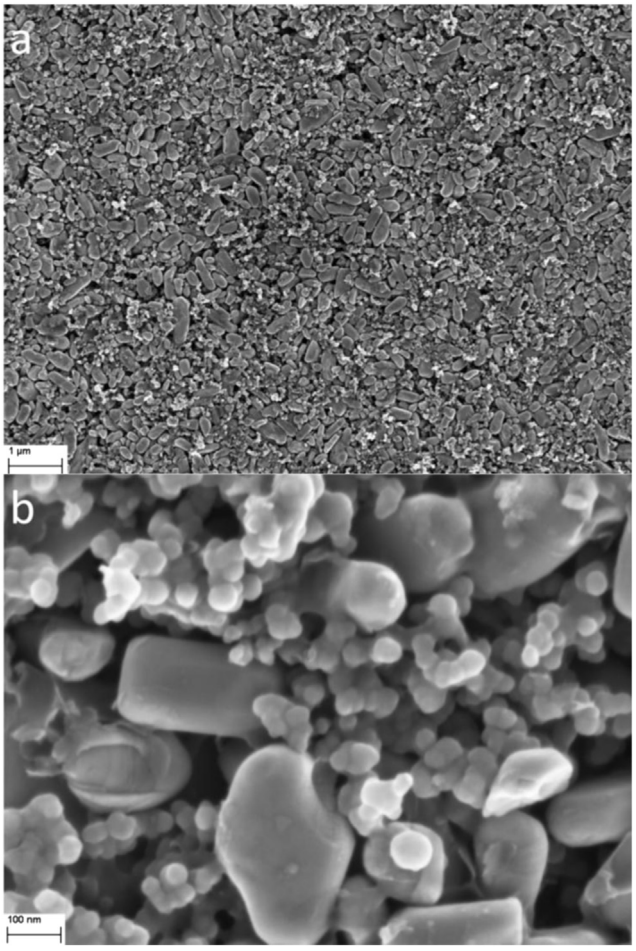

Fig. 13. (a) and (b) SEM images of a LFP/Super C65/PolyVIMTFSI-c (80/10/10 %wt) electrode.

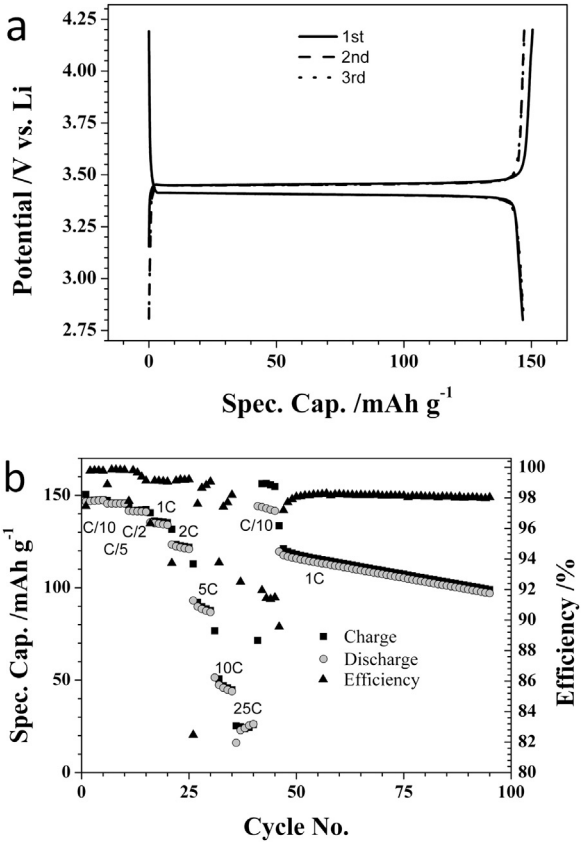

Fig. 14. (a) Voltage profiles of the two first cycles upon galvanostatic cycling of a $LiFePO_4$/SuperC65/PolyVEIMTFSI-c (80/10/10 %wt) electrode at C/10. Electrolyte: 1 M $LiPF_6$ (EC/DEC) (3/7) (v/v). Counter and reference electrodes: Li. (b) Galvanostatic cycling at various C-rates as indicated on the graph. Counter and reference electrodes: Li.

time, the proportion of parasitic reaction during lithiation is increasing. It has to be pointed out that if many articles report anodic stability for imidazolium based IL above 4.2 V, a closer look at the voltammogram [20] shows a first shoulder for EMIMFSI prior to extensive electrolyte decomposition as well as a strong decay over cycling for Li/EMIMFSI–LiTFSI/$LiCoO_2$ cells (as compared with Li/$PYR_{13}FSI$/$LiCoO_2$ cells), which indicates a lower long term anodic stability for imidazolium-based ILs as compared with pyrrolidinium-based ILs including the same anion. This is also consistent with the reported curves for EMIMTFSI [21,22] which show decomposition starting before 1.5 V vs Ag. Thus, we propose that progressively, upon cycling, some soluble decomposition products are generated at the PIL/other particles interfaces, which in turn react more and more, while the contact between particles is progressively lost.

If this is the case, it would not be inconsistent with the excellent binding of the polymer well below its expected reduction voltage in the case of graphite. Indeed, oxidation often leads to fragmentation, whereas reduction leads to radical anions often more stable and easier to polymerize at the surface of the electrode (especially in the presence of EC, which provide additional polymerizable species). This could somehow explain the poor cycling results obtained with $LiFePO_4$ especially as swelling of the particles with electrolyte (inducing losses of electronic contact for active particles), which could have been another alternative explanation should also have occurred in the case of LTO electrodes. Other cationic moiety with better stability such as cyclic or acyclic quaternary ammoniums could probably lead to improved results in case the anodic stability of the PIL is limiting.

4. Conclusion

We demonstrated the possibility of obtaining PIL nanoparticles from 1-vinyl-3-alkyl imidazolium $TFSI^-$ monomers bearing short alkyl chains, which offers a wide range of uses, considering the number of hydrophobic PILs reachable, in particular as binder in combination with small active materials for Li-batteries application. Contrary to SBR latexes, the PIL nanoparticles are not processed above their Tg and their adhesion during the electrode preparation requires their gelation during slurry preparation. However, after solvent removal the PIL nanoparticles are expected to establish rather stiff 'glue points' granting good mechanical properties.

The PIL nanoparticles were used successfully as nanolatex binder in combination with LTO to produce electrodes offering excellent delivered capacities, rate performance and long-term cycle stabilities.

Graphite electrodes made using PIL nanobinder also showed very good cycling stability with limited capacity decay. The excellent binding properties of the nanolatex might be resulting from the PIL reduction at low potentials, leading to chemical bonding of the binder to the carbon surface. However, the reduction processes lead to irreversible capacities in the first cycles that need to be addressed for use in commercial Li-ion batteries. Nevertheless, the approach is promising and improvements are expected from

decreasing the binder content and using more stable cationic moieties such as pyrrolidinium or piperidinium.

The use of PIL nanobinder in combination with LFP did not result in electrodes having acceptable long-term cycling performance despite a very high reversibility in the initial cycles. The decay has been related with the instability in oxidation of the imidazolium moiety. However, the use of more electrochemically stable moieties could result in better performing positive electrodes.

Acknowledgments

Financial support from the European Commission within the ORION project (229036) under the Seventh Framework Program (FP7) is gratefully acknowledged as well as Sachtleben Pigments Oy for providing the LTO powder.

References

[1] M. Armand, F. Endres, D.R. MacFarlane, H. Ohno, B. Scrosati, Nat. Mater. 8 (2009).
[2] Y. Bai, Y. Cao, J. Zhang, M. Wang, R. Li, P. Wang, S.M. Zakeeruddin, M. Grätzel, Nat. Mater. 7 (2008) 626.
[3] R.D. Costa, E. Orti, H.J. Bolink, Stefan Graber, C.E. Housecroft, E.C. Constable, Adv. Funct. Mater. 20 (2010) 1511.
[4] A. Balducci, W.A. Henderson, M. Mastragostino, S. Passerini, P. Simon, F. Soavi, Electrochim. Acta 50 (2005) 2233.
[5] E. Paillard, Q. Zhou, W.A. Henderson, G.B. Appetecchi, M. Montanino, S. Passerini, J. Electrochem. Soc. 156 (2009) A891.
[6] H. Ohno, Electrochim. Acta 46 (2001) 1407.
[7] R. Marcilla, M. Curri, P. Cozzoli, M. Martínez, I. Loinaz, H. Grande, J. Pomposo, D. Mecerreyes, Small 2 (2006) 507–512.
[8] G.B. Appetecchi, G.-T. Kim, M. Montanino, M. Carewska, R. Marcilla, D. Mecerreyes, I. De Meatza, J. Power Sources 195 (2010) 3668–3675.
[9] J. Yuan, M. Antonietti, Polymer 52 (2011) 1469–1482.
[10] J. Yuan, M. Antonietti, Macromolecules 44 (2011) 744–750.
[11] D. Bresser, E. Paillard, E. Binetti, S. Krueger, M. Striccoli, M. Winter, S. Passerini, J. Power Sources 206 (2012) 301–309.
[12] S.F. Lux, F. Schappacher, A. Balducci, S. Passerini, M. Winter, J. Electrochem. Soc. 157 (2010) A320.
[13] G.T. Kim, S.S. Jeong, M. Joost, E. Rocca, M. Winter, S. Passerini, A. Balducci, J. Power Sources 196 (2011) 2187.
[14] P. Bonhöte, A.-P. Dias, M. Armand, N. Papageorgiou, K. Kalyanasundaram, M. Grätzel, Inorg. Chem. 35 (1996) 1168–1178.
[15] G.B. Appetecchi, M. Montanino, M. Carewska, M. Moreno, F. Alessandrini, S. Passerini, Electrochim. Acta 56 (2011) 1300–1307.
[16] M. Montanino, M. Moreno, F. Alessandrini, G.B. Appetecchi, S. Passerini, Q. Zhou, W.A. Henderson, Electrochim. Acta 60 (2012) 163–169.
[17] G.B. Appetecchi, S. Scaccia, C. Tizzani, F. Alessandrini, S. Passerini, J. Electrochem. Soc. 153 (2006) A1685–A1691.
[18] E. Paillard, M. Bedu, M. Winter, S. Passerini, Ionic liquid monomer forming stable SEI on graphite in Pyr14TFSI-LiTFSI electrolyte, in: COIL–4, Washington DC (15–18th June 2011).
[19] A.J. Arduengo, H.V.R. Dias, R.L. Harlow, M. Kline, J. Am. Chem. Soc. 114 (14) (1992) 5530.
[20] H. Matsumoto, H. Sakaebe, K. Tatsumi, M. Kikutab, E. Ishiko, M. Kono, J. Power Sources 160 (2006) 1308–1313.
[21] A.B. McEwen, H.L. Ngo, K. LeCompte, J. Goldman, J. Electrochem. Soc. 146 (1999) 1687–1695.
[22] M. Egashira, S. Okada, J.-i. Yamaki, Solid State Ionics 148 (2002) 457–461.